buildings

Article

The Cracking and Tensile-Load-Bearing Behaviour of Concrete Reinforced with Sanded Carbon Grids

Michael Frenzel , Enrico Baumgärtel *, Steffen Marx and Manfred Curbach

Faculty of Civil Engineering, Institute of Concrete Structures, TUD Dresden University of Technology, 01062 Dresden, Germany; michael.frenzel@tu-dresden.de (M.F.); steffen.marx1@tu-dresden.de (S.M.); manfred.curbach@tu-dresden.de (M.C.)

* Correspondence: enrico.baumgaertel@tu-dresden.de; Tel.: +49-351-463-42631

Abstract: This article presents the cracking and load-bearing behaviour of carbon-reinforced prismatic concrete tensile specimens. Grids with different geometries and impregnations were used as carbon reinforcement. In addition, the roving surfaces were partially coated with a fine sand to improve the bond between concrete and reinforcement. The article shows the influence of the different parameters on the developing cracks with respect to their width and spacing from each other. The material properties and tensile strengths of carbon concrete are also presented. These can be used for calculations. A fine-grained, commercially available shotcrete was used for the investigations. Based on the tests and results described in this article, an influence of the sanded carbon grids on the crack properties (crack widths, crack spacing) could be shown in comparison to unsanded carbon grids.

Keywords: carbon reinforced concrete (CRC); CUBE; crack width; tensile test; textile; grid; carbon; load-bearing behaviour; fine grained concrete; surface modification; sanding

check for updates

Citation: Frenzel, M.; Baumgärtel, E.; Marx, S.; Curbach, M. The Cracking and Tensile-Load-Bearing Behaviour of Concrete Reinforced with Sanded Carbon Grids. *Buildings* **2023**, *13*, 2652. https://doi.org/10.3390/buildings13102652

Academic Editor: Andreas Lampropoulos

Received: 4 September 2023
Revised: 10 October 2023
Accepted: 19 October 2023
Published: 21 October 2023

1. Introduction

In September 2022, the carbon concrete composite (C^3) demonstration house "CUBE" was opened in Dresden. It is the world's first building to incorporate exclusively non-metallic reinforcements, mainly made of carbon fibres, to demonstrate their potential for creating slender, concrete-reduced, and aesthetically sophisticated structures [1–3]. A special feature of the CUBE building is the two TWIST shells that extend from the horizontal walls to the vertical ceiling [4,5]. They consist of a carbon-reinforced concrete (CRC) load-bearing inner shell, waterproofing and insulation layers, and a CRC weather shell [6,7]. The TWIST elements are designed in such a way that they are sufficiently load-bearing, serviceable, and durable. Especially for the roof cladding exposed to the weather. It was therefore important to investigate the CRC in terms of its deformation behaviour and tendency to tear. Figure 1, left, shows the building with the two 24.4 m long, up to approximately 7.9 m wide, and 440 mm thick TWIST shells and the simplified cross-sectional structure (Figure 1, right). Every TWIST element also extends beyond the building to form an 8 m long wing. It is only 60 mm thick at the wingtip.

The two TWIST elements were to be produced on site without joints and, if possible, in one pour from shotcrete. With a planned shell length of more than 24 m, this presented a challenge. It was therefore important to be able to record, estimate, and calculate the crack patterns to be expected in the load-bearing and weather shells as a reaction of the service loads and the resulting deformations as realistically as possible. Therefore, the focus of the preliminary experimental investigations was on the determination of crack widths and spacings and the definition of the material characteristics for CRC under tensile loading.

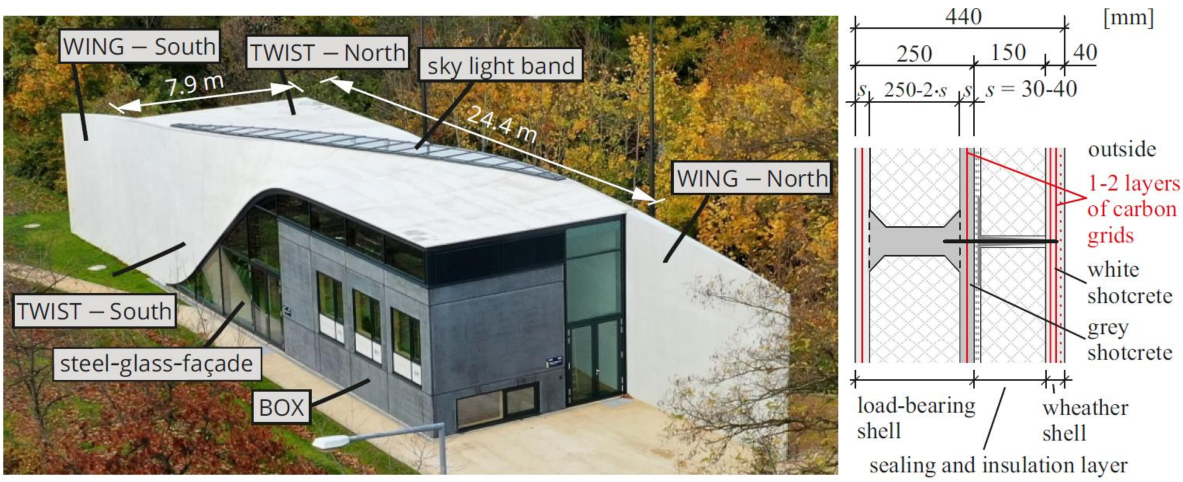

Figure 1. C^3 technology demonstration house CUBE (**left**) and standard cross section (**right**); photo: Stefan Gröschel; graphic: modified from [8].

Different experimental setups to determine the tensile-load-bearing capacity of textile reinforced concrete were carried out in 2012 by Hartig et al. [9]. A special test method was recommended by the Rilem Technical Committee in 2016 [10] which also gave the basis for the investigations of Schütze et al. in 2018 [11]. The properties of carbon reinforced concrete under tension are determined using a rectangular concrete prism with a thickness of at least 8 mm, a length longer than 500 mm, and width greater than 60 mm. These rectangular elements are reinforced with one or two layers of the textile/carbon grid. Different failure modes can appear, like delamination or tensile failure—see, e.g., [12]. In 2022, the first draft of the German guideline “Betonbauteile mit nichtmetallische Bewehrung—Concrete components with non-metallic reinforcement” was published [13]. Part 4 describes detailed information about the testing procedure for carbon-reinforced concrete under uniaxial tension. The final version will be released in 2024.

The CRC was regarded as a homogeneous composite material for this study, i.e., the force and stress distributions within the individual components of concrete and carbon reinforcement, including their composite characteristics, were not taken into account. The investigations were carried out exclusively on the composite material. Basic information on the different concretes and carbon reinforcements used in the building can be found in [14]. The CRC tensile tests were executed between 03-2019 and 04-2020, more than one year before the manufacturing of the TWIST shells. These provided an important basis for determining the most suitable carbon grid for these elements. The cracking behaviour and material property investigations were carried out on rectangular prism specimens under uniaxial tensile loading in accordance with [11].

2. Materials

The epoxy resin impregnated carbon grids Q85 and Q95 from solidian GmbH, Albstadt, Germany with the two different impregnations E1 and E2 were used for these investigations [15,16]. According to the manufacturer, there is no difference in the effect of E1 and E2 on the mechanical properties of the reinforcements. The grids were embedded in two different fine-grained concretes. By varying different parameters of the reinforcement (number of layers, mesh size, and surface treatment by sanding), the influence of these on the crack width and spacing occurring in the concrete was to be determined. The following textile grids and concretes were used:

1. Solidian Q85/85-CCE-21-E1 (briefly: Q85-E1) E1 impregnation was used for the grids until summer 2019. As this was not applicable on a large industrial scale, it has not been used since January 2020.

2. Solidian Q85/85-CCE-21-E2 (briefly: Q85-E2) In spring 2020, the E2 impregnation represented the current state of impregnation development. In terms of process optimization, E2 impregnation could be produced more cost-effectively than E1 impregnation.
3. Solidian Q95/95-CCE-38-E1 (briefly: Q95-E1) To investigate the influence of grid type on cracking, a grid with a larger mesh size (38 instead of 21 mm) and a cross-sectional area (95 instead of 85 mm^2/m) than the Q85 textile with E1 impregnation was used.
4. Sanding Sanding took place in a separate working step after textile production. The mechanical properties of the grid remained unchanged. The grains of sand (maximum grain size < 1 mm) were glued to the grid with the E1 impregnation. Figure 2 shows an example of a section of the sanded Q85/85-CCE-21-E1 (left) and the sanded Q95/95-CCE-38-E1 (right) grids.
5. Concrete C20.2 grey Grey shotcrete from PAGEL Spezial-Beton GmbH, Essen, Germany with a maximum grain size of 2 mm was used for the inner, non-visible area of the supporting shell. The concrete could be classified as class C50/60 according to [17].
6. Concrete C20 white White (light grey) shotcrete from PAGEL Spezial-Beton GmbH, Essen with a maximum grain size of 2 mm was used for both the weather shell and the visible chord of the load-bearing shell (see Figure 1, right). The concrete could also be classified in strength class C50/60 according to [17].

The properties of the grids used are compared in Table 1 and those of the concretes in Table 2.

Table 1. Properties of the textile reinforcements Q85 and Q95 according to the manufacturer's data sheet [11,12] with added weights.

Property	Unit	Q85		Q95	
		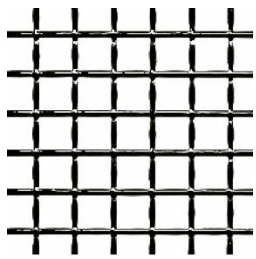			
		longitudinal	transversal	longitudinal	transversal
roving					
axis distance	mm	21	21	38	38
cross section	mm^2	1.81	1.81	3.62	3.62
grid					
cross-sectional area	mm^2/m	85	85	95	95
average tensile strength	MPa	3300	3550	3200	3300
modulus of elasticity	GPa	>220	>205	>220	>205
weight per unit area	g/m^2	ca. 540		ca. 550	
weight per unit area	g/m^2	sanded: approx. 960		sanded: approx. 1000	

Table 2. Properties of the concrete mixtures [14].

Concrete and Concrete Class	Cement	Aggregates	Fresh Concrete Density (kg/m^3)	Water/Binder Ratio [-]	Water/ Cement Ratio [-]
C20 white, C50/60	CEM I 42,5 R, white	silica sand 0/2	2200	0.34	0.32
C20.2 grey, C50/60	CEM I 52,5 N	silica sand 0/2	2200	0.35	0.32

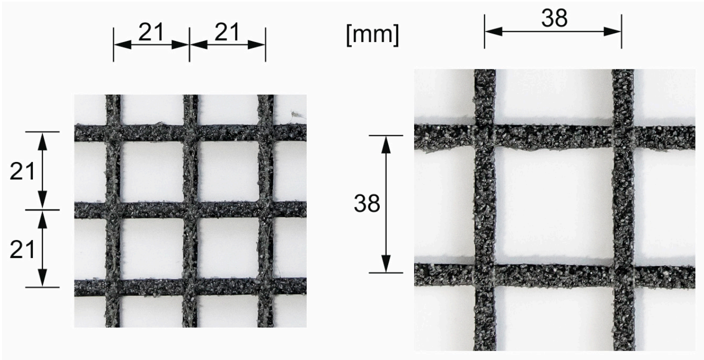

Figure 2. Cutouts from sanded carbon grids; solidian Q85/85-CCE-21-E1 (**left**) and Q95/95-CCE-38-E1 (**right**); photos: Stefan Gröschel.

To characterize the two concretes, the flexural tensile and compressive strengths at 28 days of age were determined using prisms (L/D/W: 160/40/40 mm^3) as per [18]. The flexural tensile strength and the unaxial tensile strength derivable from it were of particular interest since they play a decisive role in the cracking behaviour of the shells. The average values were 12.7 N/mm^2 (C20.2 grey) and 13.5 N/mm^2 (C20 white), respectively, after 27 days and water immersion. The uniaxial tensile strength f_{ct} was derived from the flexural tensile strength $f_{ct,fl}$, taking into account the geometry of the specimens according to [19]; in the present case, f_{ct} = 44.1% of $f_{ct,fl}$. For both concretes, significantly higher tensile strengths than specified in [20] were achieved with 5.6 N/mm^2 and 6.0 N/mm^2, respectively (f_{ctm} = 4.1 N/mm^2 and $f_{ctk;0.05}$ = 2.9 N/mm^2 for a concrete of class C 50/60).

The tensile test specimens were reinforced with one or two layers of the solidian grids. Each specimen of the six series examined had three rovings in the longitudinal direction. The middle roving was centred in the specimen. This resulted in a specimen width b_{plan} of 63 mm for the Q85 specimens and 114 mm for the Q95 specimens. With a concrete cover c_{plan} of 15 mm, the single-layer specimens had a thickness t_{plan} of 30 mm, and the double-layer specimens had a thickness of 40 mm. The specimens of series A to D had a total length L_G of 1160 mm and a free length L_F of 600 mm, see Figure 3a. On the other hand, for series E and F, the total length L_G was 800 mm, and the free length L_F was 400 mm. In all cases, the cracks and strains were measured over a measuring range L_M of 300 mm with a digital image correlation (DIC) system.

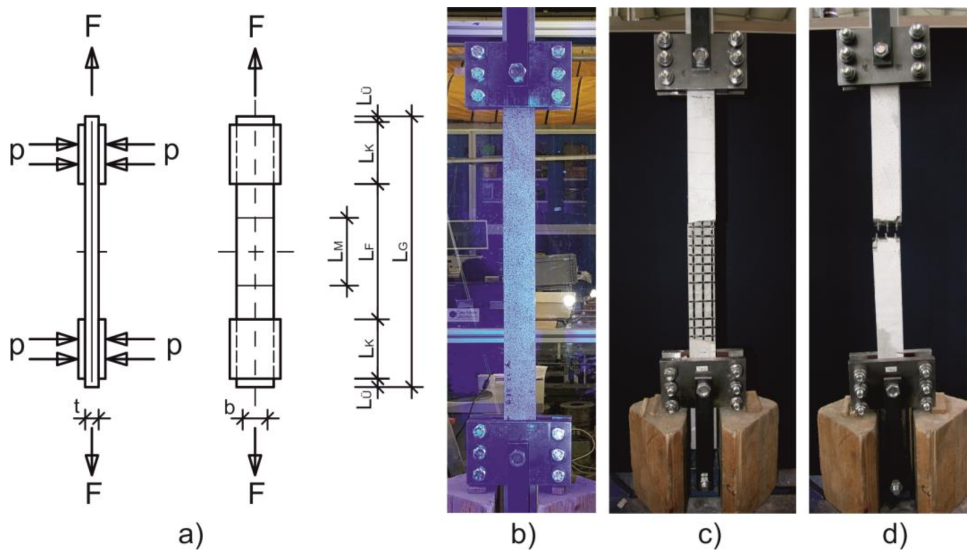

Figure 3. (**a**) Schematic testing setup; (**b**) Q85-test specimen in test rig with DIC, (**c**) delamination failure of a Q85-specimen, series A; (**d**) tensile failure of a Q85-specimen, series B; photos: Michael Frenzel.

Both the spraying and laminating methods were used to produce the test specimens. A first layer of concrete was sprayed into the formwork and removed with a gauge to achieve as much of the intended layer thickness as possible. After the grid was embedded, another layer of concrete was sprayed on top. This completely covered the textile. Depending on the number of layers, the procedure described above was repeated.

For the unconfined tensile test, the test specimens were clamped uniformly at both ends over a length L_K of 120 mm (series A to D) and 175 mm (series E and F) between steel plates via bolts or hydraulically controlled cylinders. The contact pressure F of 50 Nm or 150 bar was set so that no slipping occurs between the loading plates and the concrete specimens. The subsequent tensile loading was basically displacement-controlled with a loading rate of 0.0167 mm/s up to 10 kN (until after completion of crack formation) and then with 0.0333 mm/s until failure. A few specimens were loaded to failure at 0.0167 mm/s to determine their behaviour. During the tensile test, the data logger recorded the machine force, the machine displacement, and the change in length by means of DIC at a measuring length of 300 mm. With the help of DIC, the crack distribution and the crack widths could also be determined afterwards. For this purpose, virtual inductive displacement transducers of 5–10 mm in length were created and positioned so that they were both centred across the width of the specimen and centred above the cracks.

An overview of the six-test series carried out with a total of 27 specimens is given in Table 3. In addition to the type of concrete, the layers used, the planned and measured specimen thicknesses and widths t_{plan}/t_{prov} or t_{plan}/t_{prov}, and the concrete cover c_{plan}, the numbers of specimens and layers are also listed.

Table 3. Scope of testing, series.

Series	Concrete	Grid	Thickness t_{plan}/t_{prov} (mm)	Width b_{plan}/b_{prov} (mm)	Concrete Cover c_{plan} (mm)	Spec. (No.)	Grid Layers (No.)
A	C20 white	Q85-E1	40/35	63/62	15	5	2
B	C20 white	Q85-E1, sanded	40/35	63/62	15	5	2
C	C20 white	Q95-E1	40/37	114/112	15	2	2
D	C20 white	Q95-E1, sanded	40/36	114/112	15	3	2
E	C20 white	Q85-E2	40/42	63/62	15	5	2
F	C20.2 grey	Q85-E2	30/30	63/62	15	6	1

Each series is described in more detail below. Stress–strain curves were determined from force-displacement changes for all six series. In addition, the crack development was observed and the occurring crack widths and spacings were measured for series A–E.

A. Shows the interaction of the concrete C20 white with the textile Q85/85-CCE-21-E1. The grid was installed in two layers in the five specimens examined, which were approx. 40 mm thick, and geometrically corresponded to the reinforcement situation in the CUBE weather shell and the lower chord of the CUBE load-bearing shell. These series served as a reference.
B. The five tensile specimens investigated are configured in the same way as in series A. A sanded Q85/85-CCE-21-E1 grid was used to show whether and how the sanding affects the stress–strain curve of the grid and the crack pattern. A direct comparison with series A was therefore possible.
C. Shows the interaction of the concrete C20 white with the textile Q95/95-CCE-38-E1. The textile was also installed in two layers in three tensile specimens. By comparing the stress–strain curves and crack patterns with those of series A, it was to be shown to what extent they differ as a result of different yarn spacings and roving diameters. However, since one test had to be aborted due to technical problems, only two of the three test specimens could be evaluated.
D. The three tensile specimens were configured analogously to the C series. In these specimens, however, the sanded textile Q95/95-CCE-38-E1 was installed in order to

be able to evaluate the influence of the sanding on the textile characteristic and the crack pattern. In addition, the influence of the grid geometry could be evaluated by comparison with series B.

E. Shows the interaction of concrete C20 white with the two-layer textile Q85/85-CCE-21-E2. The comparison with reference series A was intended to show the influence of impregnation E2 on the textile working line and crack patterns.

F. The test specimens were concreted with the concrete C20.2 grey and provided with a layer of textile Q85/85-CCE-21-E2. Since this material combination was intended for the top flange of the TWIST load-bearing shell, the comparison with series E was intended to show the influence of the concrete type and number of layers on the textile characteristic curve. Finally, a crack investigation was not carried out on the six specimens of this series.

3. Constitutive Laws

3.1. Results

Figures 4–9 show the stress–strain curves of the individual test specimens for series A to F and the measured crack openings for series A to E. For this purpose, the measured tensile forces were related to the textile area (textile stress) and to the concrete gross area (concrete stress). The roving cross-sectional area A_{tex} for the Q85 series A, B, E, and F is 1.81 mm^2 and for the Q95 series C and D 3.62 mm^2. The concrete gross area is calculated from the existing specimen widths and thicknesses (b_{prov} and t_{prov}), Table 3. The strain of the specimen was obtained from the change in length of the 300 mm long centrally arranged measuring distance L_M (Figure 3). The following results and findings were obtained:

1. Course of stress–strain curves and failure modes.

Qualitatively, the courses were identical for all tensile specimens. In the first state, the specimen remains uncracked, and the curves show a linear progression (state I, see Figure 4). When the concrete’s tensile strength was reached, the specimen began to crack. With further loading, more and more cracks formed along the length of the specimen (state IIa). At this stage, the deformations of the specimen became significantly larger for small increases in load. When cracking was complete, the load was increased to failure (state IIb).

The specimen failed either due to failure of the textile–concrete bond, as evidenced by delamination or spalling of the concrete along the textile plane (interlaminar debonding) due to blast cracking, or as a result of rupture of the grid (textile tensile failure). All the tensile specimens, except those of series B, failed as a result of interlaminar debonding. An example of this is shown in Figure 3c. Tensile failure of the textile occurred in all specimens of series B. Figure 3d shows a specimen with ruptured carbon yarns.

2. Considerations in state I (uncracked concrete)

The tensile strength of the concrete is naturally subject to a higher fluctuation than the compressive strength. Due to the constant cross-sectional dimensions in the longitudinal direction of the specimen, it was not possible to predict at which point of the specimen the initial crack occurs. Furthermore, the magnitude of the initial crack force depends on the free tensile length of the specimen. The number of cracks initiating weak points in the concrete increases with the free length L_F (see Figure 3). The tensile strength of concrete is usually determined from the flexural or splitting tensile strength by probabilistic and mechanical considerations, see e.g., [21,22]. The effect can be seen by comparing series A and E (see Figures 4 and 8). For series A, the average unconfined tensile strength at a free clamping length of 600 mm is 2.7 N/mm^2, for series E with a clamping length of 400 mm the value is 37% higher at 3.7 N/mm^2. In addition, it should be mentioned that a direct tensile strength testing method for concrete is presented in [23], which could be applied for the used concretes.

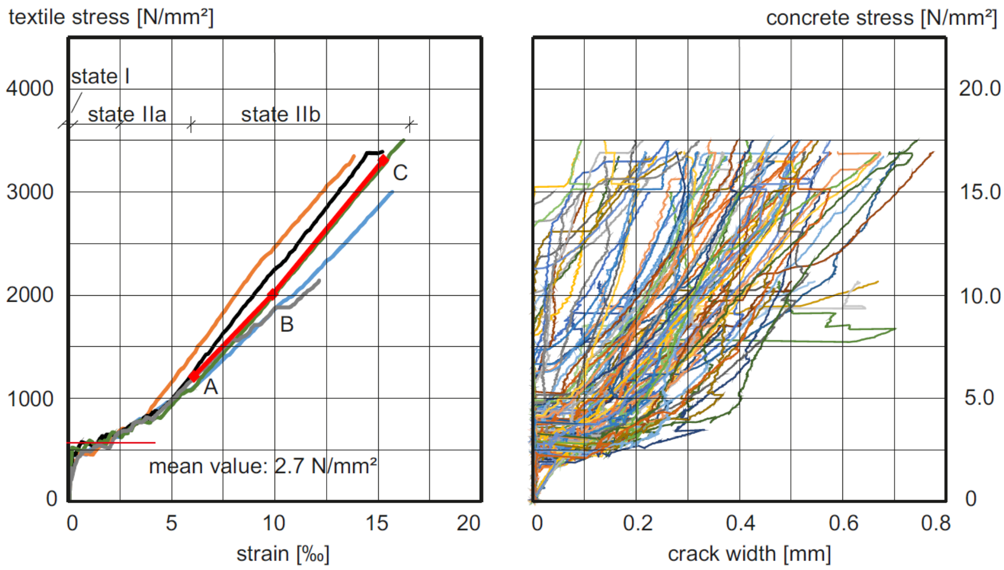

Figure 4. Stress–strain and stress–crack relations of series A, C20 white-Q85-E1, 2 layers.

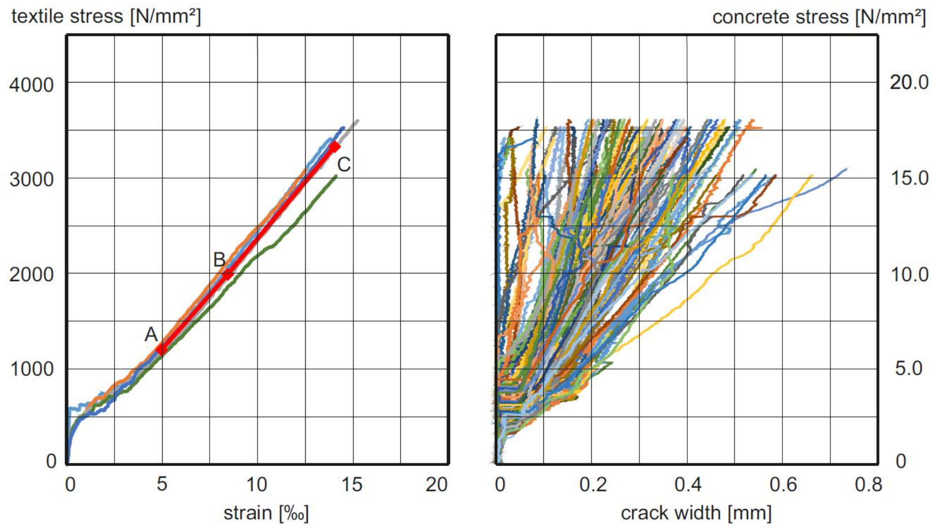

Figure 5. Stress–strain and stress–crack relations of series B, C20 white-Q85-E1, sanded, 2 layers.

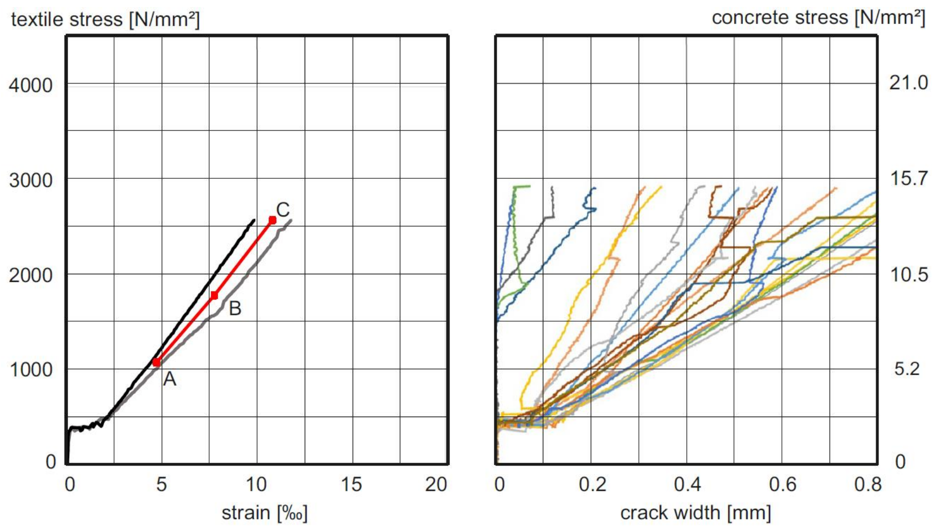

Figure 6. Stress–strain and stress–crack relations of series C, C20 white-Q95-E1, 2 layers.

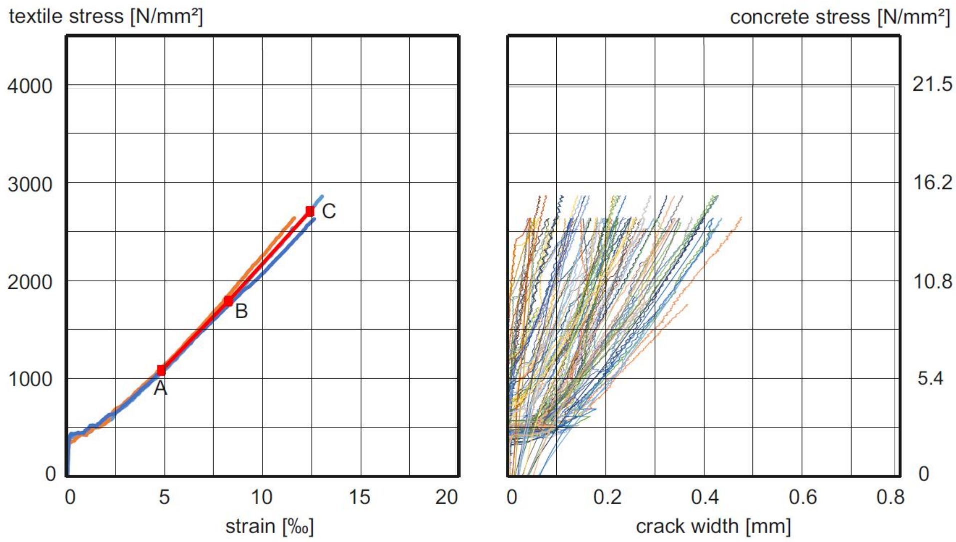

Figure 7. Stress–strain and stress–crack relations of series D, C20 white-Q95-E1, sanded, 2 layers.

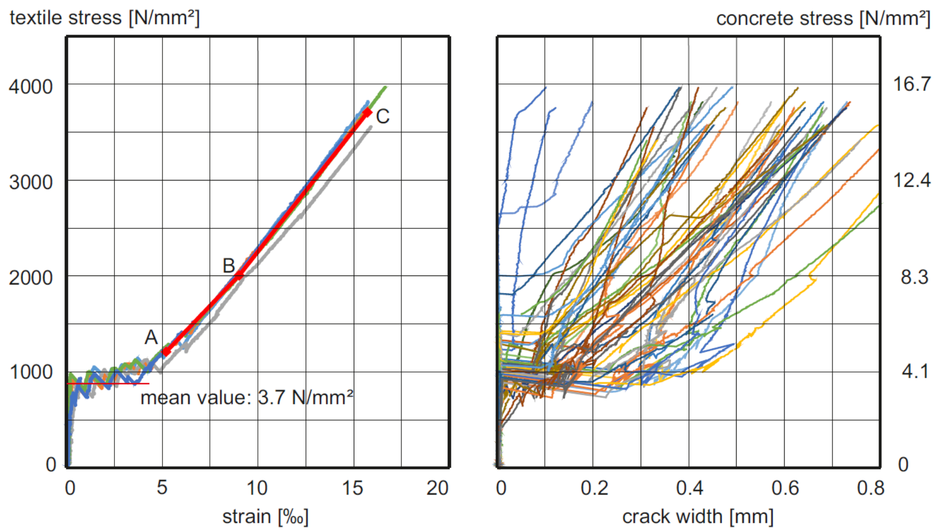

Figure 8. Stress–strain and stress–crack relations of series E, C20 white-Q85-E2, 2 layers.

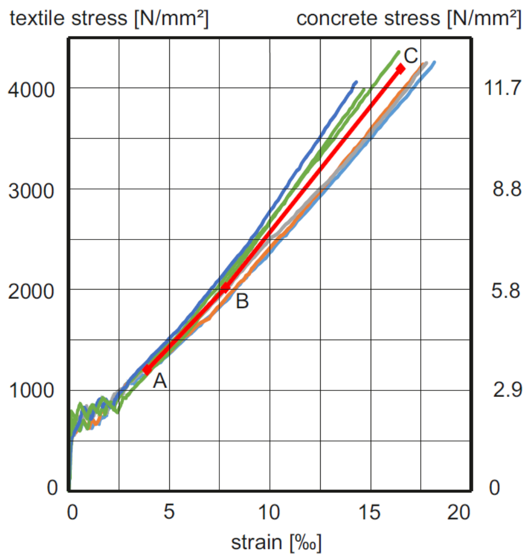

Figure 9. Stress–strain relations of series F, C20.2 grey-Q85-E2, 1 layer.

3. Considerations in state IIa/IIb (cracked concrete)

Based on the recorded stress–strain curves, the transition from state Ia to IIb could not be clearly determined. After reviewing all characteristics, the transition was set at an average textile stress σ_{tex} = 1200 N/mm^2 (point A). At this point, cracking was largely completed in all tensile specimen. Since the curve in area IIb could be better approximated bilinearly than linearly, a further evaluation point B was defined at a mean textile stress of σ_{tex} = 2000 N/mm^2. For this, the corresponding mean strain could be determined by forming the arithmetic mean of the 2–6 values per series at the stress level of 2000 N/mm^2. The mean ultimate stress and strain (point C) were also determined by arithmetic averaging of the respective individual values. The bilinear line in area IIb forms part of the material characteristic curve for carbon concrete required for calculations, which is quadrilinear taking into account states I and IIa (approximated). The line and value pairs are shown for each series in the following figures and summarized into values in Table 4. In addition, the slope of the straight line was calculated both between points A and B (AB) and B and C (BC) and between the coordinate origin and points A and B (0A, 0B), which can also be referred to as the modulus of elasticity.

Table 4. Characteristic values of the bilinear stress–strain curve in state IIb.

Series				**A Q85-E1 2 Layers**	**B Q85-E1 2 Layers Sanded**	**C Q95-E1 2 Layers**	**D Q95-E1 2 Layers Sanded**	**E Q85-E2 2 Layers**	**F Q85-E2 1 Layer**
R.	Area		(mm^2)	62 × 35	62 × 35	112 × 37	112 × 36	62 × 42	62 × 30
1	Point								
2		ε_{tex}	(‰)	6.1	5.0	4.7	4.8	5.2	3.9
3	A	σ_{tex}	(N/mm^2)	1208.0	1202.9	1209.9	1207.8	1201.4	1201.0
4		σ_c	(N/mm^2)	6.0	6.0	6.3	6.5	5.0	3.5
5		ε_{tex}	(‰)	9.9	8.4	7.8	8.3	9.1	7.8
6	B	σ_{tex}	(N/mm^2)	2003.6	1997.1	2013.9	2018.4	1999.8	2019.0
7		σ_c	(N/mm^2)	10.0	10.0	10.6	10.9	8.3	5.9
8		ε_{tex}	(‰)	15.2	14.1	10.9	12.5	15.8	16.5
9	C	σ_{tex}	(N/mm^2)	3311.0	3338.5	2911.3	3064.5	3699.5	4199.7
10		σ_c	(N/mm^2)	16.6	16.7	15.3	16.5	15.4	12.3
11		Failure mode		DF *	TF **	DF *	DF *	DF *	DF *
12	AB	E_{tex}	(N/mm^2)	207,736	228,876	259,355	234,957	207,371	209,733
13	BC	E_{tex}	(N/mm^2)	243,914	238,683	293,252	248,475	252,927	250,085
14	0A	E_{tex}	(N/mm^2)	199,664	242,032	257,426	249,545	231,038	308,740
15	0B	E_{tex}	(N/mm^2)	202,794	236,623	258,192	243,474	220,970	259,173

* DF: delamination failure. ** TF: tensile failure.

3.2. Discussion

The following findings were obtained from the tests and the material characteristic curves:

1. According to the results, the sanding has no significant influence on the ultimate strength and strain of the textile—see series A/B and C/D, lines 9 and 10—according to Table 4. The values between the two series deviate by a maximum of 0.8%.
2. The comparison of the A/B and C/D series shows that the grids Q95 have a lower strength of 8.2‰ to 12.1% compared to the grids Q85 (3311.0–3338.5 N/mm^2) with 2911.3 N/mm^2 and 3064.5 N/mm^2, respectively. The Q95 grids also have lower average ultimate strains of 10.9‰ and 12.5‰, respectively, than the Q85 grids of 15.2‰ and 14.1‰ (line 8, Table 4). This results in correspondingly higher moduli of elasticity (lines 12–15, Table 4).
3. The yarn tensile strength and thus maximum textile utilization could only be achieved with series B, which represented the most favourable material combination. How-

ever, since the delamination of series A occurred at a very high load level, at 99.2% (3311.0 N/mm^2/3338.5 N/mm^2) of series B, it could be concluded that there was already a very good bond between the unsanded Q85 reinforcement and the concrete. In addition, the concrete showed a sufficiently high tensile strength.

4. The unsanded textile Q85 with the E2 impregnation has a tensile strength of 3699.5 N/mm^2, which is 12% higher and an ultimate strain 3% lower than the grid Q85 with the E1 impregnation (comparison of series A and E, lines 8 and 9, Table 4). It is also evident that the E2 impregnation resulted in higher Young's moduli (lines 12–15).
5. The comparison of the characteristic values of series E and F shows that the stiffness of the embedded textiles in the cracked state (lines 12 and 13) is almost identical. In addition, the average ultimate stress of the specimens reinforced with a single layer is 4199.7 N/mm^2 (series F), which is significantly higher than the ultimate stress of the specimens reinforced with double layers, which is 3699.5 N/mm^2. Series F, on the other hand, has the lowest ultimate strain with 12.3‰ (line 10).
6. In addition, it was observed that the mean ultimate strengths for all series with Q85 textiles exceeded the value of 3300 N/mm^2 specified in the data sheet [15], while the mean strengths of the tensile specimen reinforced with Q95 (2911.3 N/mm^2 and 3064.5 N/mm^2) did not reach the value of 3200 N/mm^2 specified in the data sheet [16] (see also Table 1).

4. Crack Widths and Crack Spacing

4.1. Results

Figures 4–8 show the widths of all detected cracks along the 300 mm measurement range for each series as a function of textile or concrete stress. In addition, Figures 10–13 show exemplary DIC images of specimens from series A to D with their crack distributions. This allows the effect of the grid-sanding on the crack spacing and the number of cracks to be seen very clearly. The crack spacing decreases significantly for both Q85 and Q95 grids, resulting in an increase in the number of cracks. Table 5 summarizes the mean and maximum crack widths measured in the centre axis of the tensile specimen at a textile stress σ_{tex} of 1000 N/mm^2 and 1500 N/mm^2 respectively, and the mean crack spacing for series A through D. For better comparability, the percentage difference between each series is also shown. Series A is used as a reference and is thus set at 100%. The evaluation was carried out under textile stresses of 1000 N/mm^2 or 1500 N/mm^2, as mathematical estimates showed that the grids embedded in the CUBE roof would experience stresses in this range under service load.

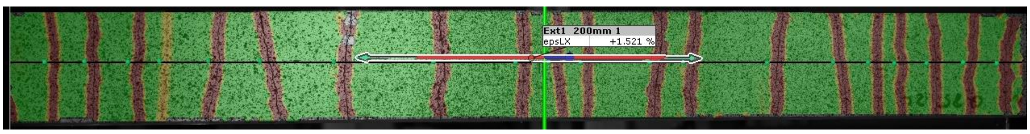

Figure 10. Cracked specimen with the carbon grid solidian Q85/85-CCE-21 E1, series A; photo: Sandra Zagermann.

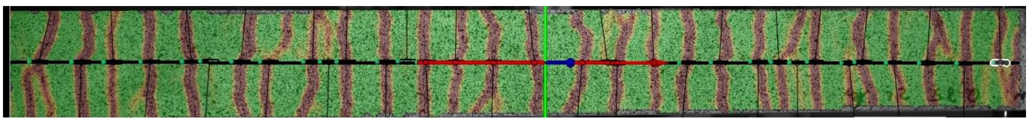

Figure 11. Cracked specimen with the sanded carbon grid solidian Q85/85-CCE-21 E1, series B; photo: Sandra Zagermann.

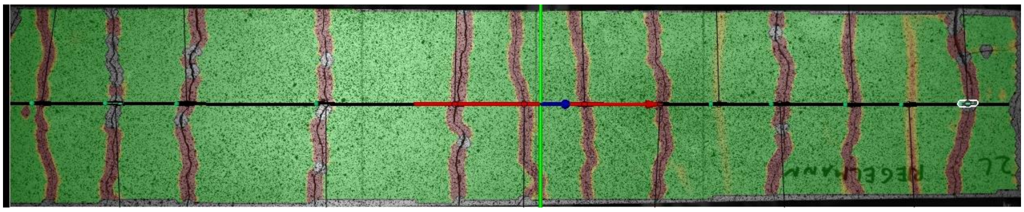

Figure 12. Cracked specimen with the carbon grid solidian Q95/95-CCE-38 E1, series C; photo: Sandra Zagermann.

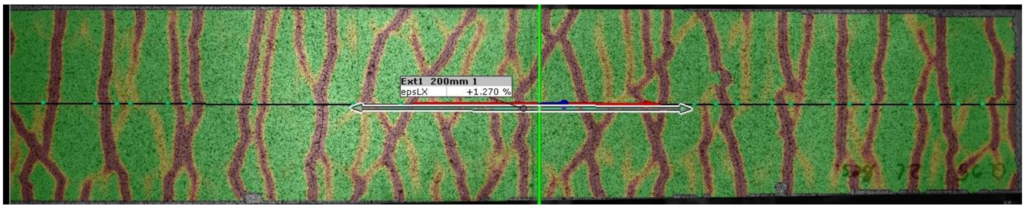

Figure 13. Crack specimen with the sanded carbon gird solidian Q95/95-CCE-38 E1, series D, photo: Sandra Zagermann.

Table 5. Comparison of crack widths and spacing for two-layer carbon reinforced tensile specimen.

Series			A Q85-E1	B Q85-E1 Sanded	C Q95-E1	D Q95-E1 Sanded	E Q85-E2
Area		(mm^2)	62 × 35	62 × 35	112 × 37	112 × 36	62 × 42
1	Free clamping length	(mm)	600	600	600	600	400
2	number of cracks per specimen	(qty)	17, 21, 22, 20, 21	28, 33, 27, 27, 25	11, 13, 11	32, 31, 28	11, 11, 10, 10, 9
3	Total number of cracks	(qty)	101	140	35	91	51
4	Average crack spacing	(mm)	30	21	86	33	39
		(%)	100	72	289	111	132
5	Mean crack opening	(mm)	0.12	0.09	0.23	0.07	0.13
	σ_{tex} = 1000 N/mm^2	(%)	100	72	185	56	101
6	Mean crack opening	(mm)	0.19	0.14	0.36	0.11	0.22
	σ_{tex} = 1500 N/mm^2	(%)	100	73	188	57	115
7	Max. crack opening	(mm)	0.40	0.23	0.28	0.08	0.40
	σ_{tex} = 1000 N/mm^2	(%)	100	58	70	20	100
8	Max. crack opening	(mm)	0.44	0.34	0.44	0.13	0.56
	σ_{tex} = 1500 N/mm^2	(%)	100	77	100	30	127

The following results were obtained from the expansion body tests with respect to crack widths and spacing:

1. Series A and E show the influence of the impregnation on the crack pattern of the Q85 specimens. The maximum crack opening is 0.44 mm for series A and 0.56 mm for E. The crack spacing increases from 30 mm to 39 mm.
2. Series A and B show that the average crack spacing and the crack width of the tensile specimen are reduced as a result of sanding. The maximum crack opening is 0.44 mm for an unsanded Q85 textile and 0.34 mm for a sanded textile. The crack spacing is reduced from 30 mm to 21 mm.
3. Series C and D: In the Q95 series investigated, sanding reduces the average crack spacing from 86 to 33 mm. The maximum crack opening is reduced from 0.44 mm to 0.13 mm.
4. The comparison of the crack spacing and crack openings between the unsanded textiles Q85 and Q95 is possible with the A and C series. Here, the crack spacing increases from 30 for the specimen reinforced with the Q85 grid to 86 mm for the

ones reinforced with the Q95 grid. The average crack opening at a textile stress σ_{tex} of 1500 N/mm^2 increases from 0.19 mm (Q85) to 0.36 mm (Q95).

5. The effect of mesh size on crack spacing and crack opening for the sanded Q85 and Q95 textiles is shown in series B and D. The test specimens with the sanded Q85 textile show a crack spacing of 21 mm, whereas the Q95 test specimens show 33 mm (see Table 5, line 4). The average crack opening at a textile stress σ_{tex} of 1500 N/mm^2 decreased from 0.14 mm (Q85) to 0.11 mm (Q95).

4.2. Discussion

The crack behaviour studies yielded the following knowledge:

1. The impregnation E2 produces a slightly weaker bond between the reinforcement and the concrete than the impregnation E1 (comparison series A and E).
2. The unsanded, finer-meshed Q85 grid results in a greater number of cracks and smaller crack widths compared to the Q95 grid.
3. The sanding of the yarn surface causes a reduction in crack spacing and crack width for both Q85 and Q95 grids. This positive effect is greater for the Q95 grid than for the Q85 grid. Table 5 shows this, for example, in the relative crack growth due to sanding. It is 38.6% (141/101, series B/A) for the Q85 grid and 160% (91/35, series D/C) for Q95 grid. The effect results from the greater yarn diameter and circumference of the Q95′s rovings compared to the Q85′s yarns.
4. The bond between the Q95 grids and the concrete is increased by sanding to such an extent that smaller average and maximum crack widths were obtained at the two stress levels investigated than for sanded Q85 grids. However, it has to be taken into account that only two specimens reinforced with the Q95 grid were available for evaluation. On the other hand, five sanded specimens reinforced with the Q85 grid could be tested (see Table 3).

5. Conclusions, Determinations and Outlook

The following conclusions were drawn from the investigations and specifications were made for the choice of reinforcement and the material properties to be used in the calculations:

1. Based on the results and the availability in principle, the textile grid solidian Q85/85-CCE-21-E2 was used for the weather shell of the CUBE-TWIST elements. It was used with an unsanded surface for the weather-protected, interior load-bearing shell (see Figure 1, right). The sanded version was used exclusively for the weather shell to ensure low crack spacing and width. It was also found that the Q85 grid was easier to form into the required curved shape of the TWIST elements than the Q95 grid, which was also an argument in favour of choosing this one.
2. According to [20], the crack widths of reinforced concrete components must be limited in such a way that their proper, permanent use is ensured with an acceptable appearance. Depending on the exposure class, maximum permissible (calculated) crack widths of 0.4 mm for interior components and 0.3 mm for exterior components are recommended. If a permissible crack width of 0.4 mm is applied for the interior load-bearing shell, the Q85-E2 textile stresses in the service condition should not exceed 1000 N/mm^2 (see Table 5, Series E). If a maximum crack opening of 0.3 mm is accepted for the outer weather shell, the stress of the sanded Q85-E2 textile should not exceed 1175 N/mm^2. This value is obtained by linear interpolation assuming that the maximum crack opening of carbon concrete with sanded Q85-E2 grids based on the results of series A/B are 0.23 mm at a textile stress of 1000 N/mm^2 and 0.43 mm (77% of 0.56 mm) at 1500 N/mm^2. However, since the carbon reinforcement is assumed not to corrode, crack widths greater than 0.3 and 0.4 mm are also permissible in terms of durability.
3. On the basis of the test results from the series E and the normative specifications for a concrete of the strength class C50/60, the quadrilinear material characteristic curve

shown in Figure 14 was constructed for the carbon-reinforced concrete investigated and used for calculations. It is defined by the points 0 to 4.

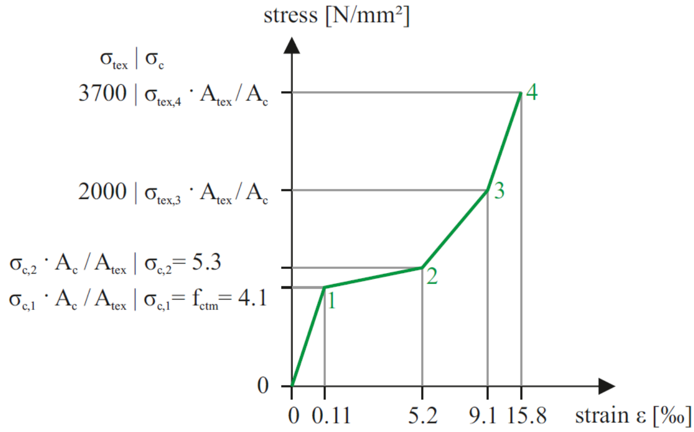

Figure 14. Quadrilinear stress–strain relation for calculations (not to scale).

- In state I (points 0–1), the standardized average tensile strength and the modulus of elasticity are used (f_{ctm} = 4.1 N/mm^2, E_{cm} = 37,000 N/mm^2).
- Point 2 defines the end of state IIa. From the series E tests, the textile strain ε_{tex} was taken to be 5.2 ‰ (see Table 4, line 2). The corresponding concrete tensile stress is set at 1.3 f_{ctm} and thus at 5.3 N/mm^2, based on the specifications of [22].
- Points 3 and 4 correspond to points B and C, respectively, of series E (see Table 4, lines 5, 6, 8, and 9).

The material characteristic curve is shown in such a way that either the textile stresses σ_{tex} or the concrete tensile stresses σ_c are indicated on the ordinate. When creating the curve, the reinforcement area A_{tex} and concrete gross area A_c must be taken into account accordingly. It should be noted that in the final building design, an ultimate stress of 3600 N/mm^2 instead of 3700 N/mm^2 was applied, see [11].

This paper shows the basis on which the stress–strain curve of carbon reinforced concrete can be determined, which was required for the design of the building and the necessary approvals, in particular the individual approval required for the CUBE building [19,24–26]. It also indicates the positive effect that sanding the yarn surface can have on crack formation. The results confirm the investigations of [27,28] on a Q85 textile, which showed that a sanded textile has a 1.5-times-higher number of cracks with 50% smaller crack spacing and up to 30% smaller crack widths compared to the same unsanded textile. Furthermore, higher tensile strengths were found with the sanded textile. This can be attributed to the improved bonding behaviour.

The crack development on the two CUBE-TWIST elements is currently being continuously monitored. For this purpose, roof inspections and crack width measurements are carried out regularly at selected, decisive points. In this way, the real crack pattern can be compared with the calculated one. Nevertheless, more extensive tensile tests should be carried out in the future to assess cracking. In addition, the effects of temperature changes and long-term stress on the yarns should be considered, as should tensile stresses that do not explicitly occur in the longitudinal direction of the yarn.

Author Contributions: Conceptualization, M.F.; methodology, M.F.; validation, M.F.; formal analysis, M.F.; investigation, M.F.; data curation, M.F.; writing—original draft preparation, E.B. and M.F.; writing—review and editing, E.B. and M.F.; visualization, E.B. and M.F.; supervision, M.C. and S.M.; project administration, M.C. and S.M.; funding acquisition, M.C. and S.M. All authors have read and agreed to the published version of the manuscript.

Funding: This research was funded by Federal Ministry of Education and Research, grant number 03ZZ0309A.

Data Availability Statement: Data are contained within the article.

Acknowledgments: The authors would like to thank all the parents involved in the project and the colleagues at the Otto Mohr Laboratory for their support and good cooperation.

Conflicts of Interest: The authors declare no conflict of interest.

References

1. Curbach, M. (Ed.) *CUBE: Neues Bauen mit Carbonbeton | New Building with Carbon Concrete*; Wasmuth & Zohlen: Berlin, Germany, 2022; ISBN 9783803023728.
2. Tietze, M.; Frenzel, M.; Curbach, M. C3 technology demonstration house—CUBE. In Proceedings of the 18th fib Symposium, Lisbon, Portugal, 14–16 June 2021; Júlio, E., Valença, J., Louro, A.S., Eds.; fib (The International Federation for Structural Concrete): Lausanne, Switzerland, 2021; pp. 153–162.
3. *CUBE Das Carbonbetongebäude S2*; Ernst & Sohn: Berlin, Germany, 2023; pp. 1–143. Available online: https://onlinelibrary.wiley.com/toc/14371006/2023/118/S2 (accessed on 18 October 2023).
4. Vakaliuk, I.; Frenzel, M.; Curbach, M. Application of parametric design tools for the roof of the C^3 technology demonstration house—CUBE. In Proceedings of the IASS Annual Symposia 2019—Form and Force, Barcelona, Spain, 7–10 October 2019; Lázaro, C., Bletzinger, K.-U., Oñate, E., Eds.; International Association for Shell and Spatial Structures (IASS): Guildford, UK, 2019; pp. 1077–1084.
5. Vakaliuk, I.; Frenzel, M.; Curbach, M. C^3 technology demonstration house CUBE, "From digital model to realization". In Proceedings of the IASS Annual Symposia 2020/21 and the 7th International Conference on Spatial Structures, Guilford, UK, 23–27 August 2021; Behnejad, S.A., Parke, G.A.R., Samavati, O.A., Eds.; International Association for Shell and Spatial Structures (IASS): Guildford, UK, 2022; pp. 1827–1837. [CrossRef]
6. Frenzel, M.; Tietze, M.; Curbach, M. C^3 technology demonstration house: CUBE: Design and manufacturing of the twisted roof-wall construction. In Proceedings of the 6th fib International Congress 2022, Oslo, Norway, 12–16 June 2022; Stokkeland, S., Braarud, H.C., Eds.; pp. 2542–2550.
7. Zavadski, V.; Frenzel, M. Aufbau, Bemessung und Planung der TWIST- Carbonbetonschalen. In *Beton- und Stahlbetonbau 118, Sonderheft CUBE Das Carbonbetongebäude S2*; Ernst & Sohn: Berlin, Germany, 2023; pp. 71–81. [CrossRef]
8. Stelzmann, M.; Frenzel, M.; Holschemacher, K. Herstellung von Carbonbetonbauteilen im Spritzverfahren—Technologieentwicklung. *Beton-Und Stahlbetonbau* **2023**, *118*, 92–101. [CrossRef]
9. Hartig, J.; Jesse, F.; Schicktanz, K.; Häußler-Combe, U. Influence of experimental setups on the apparent uniaxial tensile load-bearing capacity of Textile Reinforced Concrete specimens. *Mater. Struct.* **2012**, *45*, 433–446. [CrossRef]
10. Brameshuber, W. Recommendation of RILEM TC 232-TDT: Test Methods and Design of Textile Reinforced Concrete: Uniaxial Tensile Test: Test Method to Determine the Load Bearing Behavior of Tensile Samples Made of Textile Reinforced Concrete. *Mater. Struct.* **2016**, *49*, 4923–4927. [CrossRef]
11. Schütze, E.; Bielak, J.; Scheerer, S.; Hegger, J.; Curbach, M. Einaxialer Zugversuch für Carbonbeton mit textiler Bewehrung. *Beton-Und Stahlbetonbau* **2018**, *113*, 33–47. [CrossRef]
12. Mattarollo, G.; Randl, N.; Pauletta, M. Investigation of the Failure Modes of Textile-Reinforced Concrete and Fiber/Textile-Reinforced Concrete under Uniaxial Tensile Tests. *Materials* **2023**, *16*, 1999. [CrossRef] [PubMed]
13. DAfStb-Richtlinie (Draft)—Betonbauteile mit nichtmetallischer Bewehrung; Teil 1: Bemessung und Konstruktion; Teil 2: Bewehrungsprodukte; Teil 3: Hinweise zur Bauausführung; Teil 4: Empfehlungen für Prüfverfahren; Teil 5: Hinweise zu erforderlichen Nachweisen für die Verwendbarkeit der Bauprodukte (nichtmetallische Bewehrung) und der Anwendbarkeit der Bauart. *November 2022, 214 Seiten.* Available online: https://www.beuth.de/en/draft-technical-rule/dafstb-betonbauteile-nichtmetallische-bewehrung/362887890 (accessed on 18 October 2023).
14. Frenzel, M.; Scheerer, S.; Schmidt, A. Übersicht über die im CUBE verwendeten Materialien. *Beton-Und Stahlbetonbau* **2023**, *118*, 25–36. [CrossRef]
15. solidian GmbH (2019) solidian Q85/85-CCE-21 [Technical Data sheet]. Available online: https://solidian.com/wp-content/uploads/solidian-GRID-Qxx-CCE-xx-Technical-Product-Data-Sheets-v2302.pdf (accessed on 18 October 2023).
16. solidian GmbH (2019) solidian Q95/95-CCE-38 [Technical Data sheet]. Available online: https://solidian.com/wp-content/uploads/solidian-GRID-Qxx-CCE-xx-Technical-Product-Data-Sheets-v2302.pdf (accessed on 18 October 2023).
17. *DIN 1045-2:2008-08*; Tragwerke aus Beton, Stahlbeton und Spannbeton—Teil 2: Beton—Festlegung, Eigenschaften, Herstellung und Konformität—Anwendungsregeln zu DIN EN 206-1. German Institute for Standardisation (Deutsches Institut für Normung): Berlin, Germany, 2008.
18. *DIN EN 196-1:2016-11*; Prüfverfahren für Zement—Teil 1: Bestimmung der Festigkeit; Deutsche Fassung EN 196-1: 2016. Beuth: Berlin, Germany, 2016.
19. Zilch, K.; Zehetmaier, G. *Bemessung im konstruktiven Betonbau: Nach DIN 1045-1 und DIN EN 1992-1-1*; Springer: Berlin/Heidelberg, Germany, 2010. [CrossRef]
20. *DIN EN 1992-1-1:2011-01*; Eurocode 2: Bemessung und Konstruktion von Stahlbeton- und Spannbetontragwerken—Teil 1-1: Allgemeine Bemessungsregeln und Regeln für den Hochbau; Deutsche Fassung EN 1992-1-1:2004 + AC:2010 (Norm DIN EN 1992-1-1). Beuth Verlag GmbH: Berlin, Germany, 2011.

21. Bethge, W.; Richter, T. (Eds.) Schriftenreihe der Zement- und Betonindustrie. In *Beton—Prüfung nach Norm (12., überarb. Aufl.)*; Bau + Technik: Wuppertal, Germany, 2011.
22. Malárics, V. *Ermittlung der Betonzugfestigkeit aus dem Spaltzugversuch an zylindrischen Betonproben*; Institut für Massivbau und Baustofftechnologie: Karlsruhe, Germany, 2011; ISBN 978-3-86644-735-6.
23. Nilimaa, J.; Nilforoush, R. A Direct Tensile Strength Testing Method for Concrete from Existing Structures. *CivilEng* **2023**, *4*, 333–344. [CrossRef]
24. Curbach, M.; Schmidt, A.; Frenzel, M. *Antrag auf Zustimmung im Einzelfall—Ergebnishaus des C^3-Projektes—CUBE: TWIST, TU Dresden*; Institut für Massivbau: Dresden, Germany, 2020.
25. Schmidt, A.; Frenzel, M.; Scheerer, S. Schwinduntersuchungen zu einer fugenlosen 24,4 m langen Carbonbetonschale—ZiE TWIST. *Beton-Und Stahlbetonbau* **2023**, *118*, 82–91. [CrossRef]
26. Frenzel, M.; Schmidt, A.; Scheerer, S. ZiE für Carbonbetonbauteile in Halbfertigteil- und Fertigteilbauweise im Gebäudeteil BOX des CUBE. *Beton-Und Stahlbetonbau* **2023**, *118*, 49–56. [CrossRef]
27. Morales Cruz, C.; Raupach, M. Influence of the surface modification by sanding of carbon textile reinforcements on the bond and load-bearing behavior of textile reinforced concrete. *MATEC Web Conf.* **2019**, *289*, 04006. [CrossRef]
28. Morales Cruz, C. Crack-Distributing Carbon Textile Reinforced Concrete Protection Layers: Rissverteilende Textilbeton Schutzschichten mit Textiler Carbonbewehrung. Ph.D. Thesis, RWTH Aachen University, Aachen, Germany, 2020. [CrossRef]